$5d$-level energies of Ce^{3+} and the crystalline environment. III. Oxides containing ionic complexes

P. Dorenbos
Interfaculty Reactor Institute, Delft University of Technology, Mekelweg 15, 2629 JB Delft, The Netherlands
(Received 9 January 2001; revised manuscript received 14 May 2001; published 10 September 2001)

Information on the energy of $5d$ levels of Ce^{3+} ions coordinated by CO_3^{2-}, SO_4^{2-}, PO_4^{3-}, BO_3^{3-}, and SiO_4^{4-} ionic complexes or by neutral water molecules in oxide compounds will be presented and systematically analyzed. The average energy of the $5d$ configuration of excited Ce^{3+} is shifted towards lower energy relative to the free ion value. This centroid shift depends on the binding strength of the oxygen ligands in these ionic complexes. It will be analyzed by means of a model which provides a parameter that is directly related to the polarizability of the oxygen ligands. A qualitative relationship with the electronegativity of the cations in the compounds will be demonstrated. Crystal-field splitting of the $5d$ levels is interpreted in terms of the type and size of anion polyhedron coordinating the Ce^{3+} ion. All data indicate that crystal-field splitting behaves independently from the centroid shift. By combining centroid shift and crystal-field splitting, the redshift of the first electric dipole-allowed fd transition in Ce^{3+}-doped oxide compounds will be interpreted.

DOI: 10.1103/PhysRevB.64.125117 PACS number(s): 78.55.Hx, 71.70.Ch, 78.40.−q

I. INTRODUCTION

The energy of the $5d$ excited states of the trivalent lanthanides and their location relative to those of the $4f^n$ configuration is important for the luminescence properties of lanthanide activated phosphors. Knowledge, both phenomenological and theoretical, on the relation between these $5d$ level positions and the crystalline environment will be helpful in the search for new phosphors. This has been the main motivation to collect experimental data on the $5d$-level energies of the trivalent lanthanides in inorganic compounds. Information available on all 13 lanthanides and about 350 different compounds was compiled in Refs. 1 and 2. Due to a strong $5d$-electron lattice interaction, the first dipole-allowed fd transition is lowered relative to the free ion value by an amount defined as the spectroscopic redshift $D(A)$.

The redshift, by definition zero for the free ion, varies from as low as 10 900 cm^{-1} for the lanthanide ion on the Sr^{2+} site in $SrAl_{12}O_{19}$ up to values of 31 000 cm^{-1} for Sc_2O_3. It appears approximately the same for all 13 lanthanide ions if in the same host crystal. To understand the large variation, one can entirely concentrate on Ce^{3+}-doped materials. Of all trivalent lanthanides most information is available on Ce^{3+}. Furthermore, it contains only one optically active electron resulting in the simplest energy-level structure and spectroscopy of all trivalent lanthanides.

When Ce^{3+} is in a crystal, the mean energy of the $5d$ configuration is shifted downwards relative to the free ion value. In addition, the $5d$ levels are split into at most five different crystal-field components. As a net effect the lowest energy $5d$ level is further shifted downwards. The total shift $D(A)$ can be written as[3]

$$D(A)=\epsilon_c(A)+\frac{\epsilon_{\mathrm{cfs}}(A)}{r(A)}-1890\ \ \mathrm{cm}^{-1}, \tag{1}$$

where the centroid shift $\epsilon_c(A)$ is the lowering of the average (centroid) of the five $5d$ levels. The crystal-field splitting $\epsilon_{\mathrm{cfs}}(A)$ is defined as the energy difference between the lowest and highest $5d$ level. A fraction $1/r(A)$ contributes to the redshift. $r(A)$ is usually between 1.7 and 2.4.

In Refs. 3 and 4, a model based on the instantaneous polarization of the anion ligands by the $5d$ electron[5] was used to interpret the observed centroid shift in halide compounds. This ligand polarization model relates the centroid shift ϵ_c (cm^{-1}) to the N coordinating anion ligands around Ce^{3+} via

$$\frac{\epsilon_c}{N}=\frac{1.44\times10^{17}\alpha_{\mathrm{sp}}}{R_{\mathrm{eff}}^6}, \tag{2}$$

where R_{eff} is defined as

$$\frac{1}{R_{\mathrm{eff}}^6}\equiv\frac{1}{N}\sum_{i=1}^{N}\frac{1}{\left(R_i-\frac{1}{2}\Delta R\right)^6}. \tag{3}$$

R_i (pm) are the bondlengths to the ligands in the unperturbed lattice. ΔR is the difference in ionic radius of Ce^{3+} with the cation it substitutes for. To account roughly for lattice relaxation it is assumed that the neighboring anions relax outward or inward by just half this difference. Since ligand polarization is not the only mechanism leading to centroid shift, one should treat the so-called *spectroscopic polarizability* α_{sp} ($Å^3$) as a phenomenological parameter. It is related to the average polarizability of the N nearest-neighbor oxygen ions around Ce^{3+}, but also to the average covalency between Ce^{3+} and the ligands. Most appealing of the model is the absence of fitting parameters. α_{sp} is obtained directly from the centroid shift and the crystal structure.

This paper is the next in a series of papers where the relationship between centroid shift, crystal-field splitting, and redshift with the type of crystalline environment is systematically studied. In Refs. 3 and 4, hereafter referred to as Part I and Part II, the fluoride, chloride, bromide, and iodide compounds were studied. In this work, the sulfates, carbonates, phosphates, hydrated compounds, borates, and silicates

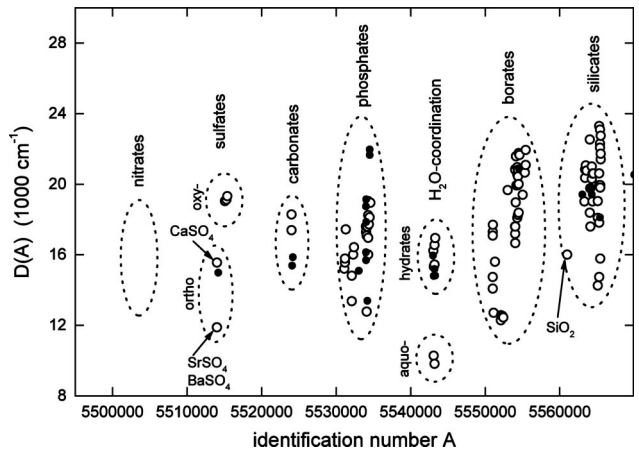

FIG. 1. Redshift $D(A)$ in oxide compounds containing ionic complexes. ●: values estimated from df emission wavelengths.

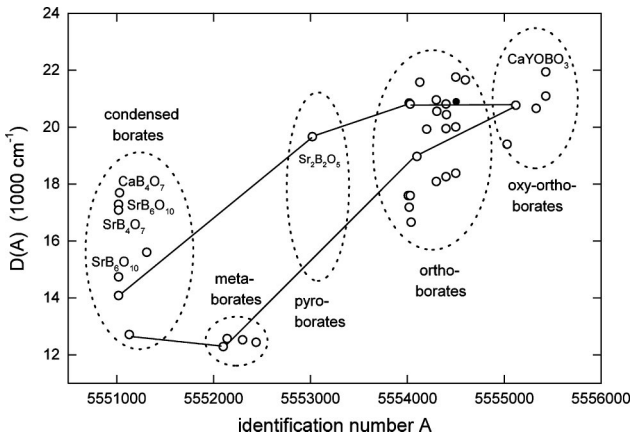

FIG. 2. Redshift $D(A)$ in borate compounds. ●: values estimated from df emission wavelengths. Data belonging to $CaLaB_7O_{13}$, LaB_3O_6, $LaBO_3$, and $SrLaOBO_3$ are connected by solid lines. Data belonging to SrB_4O_7, $Sr_2B_2O_5$, $Sr_3(BO_3)_2$, and $SrLaOBO_3$ are connected by solid lines.

are the subject of study. After the presentation of the available experimental data, the crystal-field splitting and its relationship with crystal structure will be analyzed. Crystal-field strength at the Ce^{3+} site depends on the shape and size of the first anion coordination polyhedron around Ce^{3+}. It will be shown that it is not significantly influenced by the nature of the ligands. Next, the centroid shift will be analyzed by means of the ligand polarization model. Complexes that strongly bind the oxygen $2p$ electrons like in the sulfates yield small values for α_{sp}. α_{sp} appears significantly larger for the silicates where the $2p$ electrons are less strongly bonded. Systematic behavior with the type of cations present in the compound will be demonstrated. With the results on the discussion of crystal-field splitting and centroid shift, finally the observed redshift of the full collection of compounds will be treated. It will be shown that the position of $5d$ levels in the compounds behaves in a quite predictable manner.

II. DATA ON 5*d*-LEVEL POSITIONS

A. Spectroscopic redshift

Figure 1 shows the redshift values $D(A)$ known for oxide compounds. To each compound, a seven-digit identification number A was assigned in Ref. 2. Treated as a variable, the identification number enables one to display and analyze the data in an orderly manner. On the scale in Fig. 1, the third digit (d_3), which represents the type of ionic complexes present in the crystal structure, is of significance.

Information on $5d$-level energies in the nitrates seems not to be available, and it is very scarce for the sulfates and carbonates. Much more data are available for the phosphate, borate, and silicate compounds. Figure 2, which is an expanded view of part of Fig. 1, shows the values for the redshift known for the borate compounds. On the scale in Fig. 2, the fourth digit d_4 is of significance. Its value depends on the oxygen to boron O/B ratio, and it is a representative of the amount of condensation between the borate complexes in the compound. Figure 2 shows that on average the redshift increases with decreasing amount of condensation between the borate groups. This is demonstrated by the data belonging to the La-based borates and the Sr-based borates which are connected by solid and dashed lines, respectively.

B. Centroid shift and crystal-field splitting

To obtain the centroid shift and crystal-field splitting for the Ce^{3+} $5d$ levels, information is needed on all its five $5d$-level energies. From analyzing literature data and new experiments, that information was obtained for many Ce^{3+}-doped compounds. Information is gathered in Table I. References to the literature on crystal structure will generally not be provided; they can often be found in the International Crystal Structure Database (ICSD) of FIZ Karlsruhe, Germany. From the crystal structure, the anion coordination number N and average Ce^{3+} to oxygen bond length R_{av} was obtained (see column 2).

Column 3 shows the type of anion coordination polyhedron around Ce^{3+} together with the site symmetry. Occasionally as in $LaPO_4$ and $LaBO_3$, the polyhedron is very irregular with all bond lengths different. In the case of $Lu_2Si_2O_7$ the interpretation of the 278-nm band in the excitation spectrum of Ce^{3+} luminescence is not fully certain. It introduces a slightly larger error in ϵ_c. There are two different Lu sites in the oxyorthosilicate Lu_2SiO_5. One site has sixfold, the other has sevenfold coordination. The data in Table I are for Ce^{3+} on the site yielding the smallest redshift. It is assumed that this is the site with sevenfold coordination. Four excitation bands were observed for $Li_6Y(BO_3)_3$ and it is not known where the fifth band is hidden. The resulting uncertainty in the value for the centroid shift is about 1000 cm^{-1}. Information is also incomplete for $CaCO_3$ and several other borates in Table I.

Some representative data from Table I are displayed in Fig. 3. A first inspection shows that ϵ_c in borates and silicates appears several 1000 cm^{-1} larger than in sulfates and phosphates. ϵ_{cfs} varies wildly from compound to compound and its contribution to the redshift $D(A)$ is more important than that of ϵ_c.

TABLE I. Spectroscopic and crystallographic properties of Ce^{3+}-doped compounds. (N:R_{av}) represents anion coordination number and average distance to the anions (pm). Type of polyhedron (poly) and point symmetry (sym) at the Ce site are given. Wavelengths between brackets are still uncertain.

Compound	(N:R_{av})	(poly:sym)	λ_5, λ_4, λ_3, λ_2, λ_1 (nm)	ϵ_c (cm^{-1})	ϵ_{cfs} (cm^{-1})	Ref.
$BaSO_4$	(12:295)	(irreg:C_s)	204, 215, 231, 247, 267	7880	11 600	33
$SrSO_4$	(12:282)	(irreg:C_s)	205, 214, 230, 248, 267	7880	11 300	33
$CaSO_4$	(8:247)	(ddh:C_2 or D_2)	193, 218, 238, 251, 295	8540	17 900	33
$CaCO_3$	(6:236)	(octa:C_{3i})	–, –, 245, 285, 313			34
LaP_5O_{14}	(8:250)	(ddh:C_1)	197, 208, 220, 236, 293	7070	16 600	35,36
CeP_5O_{14}	(8:248)	(ddh:C_1)	197, 208, 221, 237, 296	7220	17 000	35
LaP_3O_9	(8:253)	(ddh:C_2)	194, 205, 229, 265, 290	7990	17 100	13
$LaPO_4$	(10:264)	(irreg:C_1)	206, 214, 239, 256, 274	8660	11 900	37,13
$K_3La(PO_4)_2$	(9:≈266)[a]	(irreg:C_1)	181, 210, 246, 270, 310	8670	23 000	38
YPO_4	(8:234)	(ddh:D_{2d})	203, 225, 238, 250, 323	9570	18 010	39,40
$LuPO_4$	(8:230)	(ddh:D_{2d})	198, 225, 238, 251, 323	9670	19 600	41
$La(C_2H_5SO_4)_3\times 9H_2O$	(9:256)	(3ctp:C_{3h})	199, 211, 223, 238, 256	6460	11 200	42
aqueous-$[Ce(OH_2)_9]^{3+}$	(9:≈254)[b]	(3ctp:≈D_{3h})	199, 211, 223, 238, 253	6420	10 700	10,42
LaB_3O_6	(10:261)	(irreg:C_2)	204, 219, 246, 260, 270	8990	12 000	13
$LaMgB_5O_{10}$	(10:261)+(2:367)	(irreg:C_1)	202, 225, 239, 257, 272	8950	12 700	43,44
GdB_3O_6	(10:252)	(irreg:C_2)	205, 219, 246, 260, 270	9050	11 700	13
$YMgB_5O_{10}$	(10:≈247)+(2:≈353)[c]	(irreg:C_1)	202, 227, 235, 255, 270	8730	12 600	44
$GdAl_3(BO_3)_4$	(6:234)+(6:307)	(tp:D_3)	200, 209, 255, 278, 320	10 300	18 700	45
$YAl_3(BO_3)_4$	(6:230)+(6:306)	(tp:D_3)	200, 210, 253, 272, 322	10 200	18 900	45
$Li_6Y(BO_3)_3$	(8:240)[d]	(ddh:C_1)	217, 240, ??, 305, 346	≈12 700	17 200	44
$LuAl_3(BO_3)_4$	(6:≈226)+(6:≈302)[e]	(tp:D_3)	200, 209, 250, 269, 323	10 000	19 000	45
$LaBO_3$	(9:260)	(irreg:C_s)	215, 232, 241, 266, 330	11 500	16 200	13
$GdBO_3$	(8:240)	(2ctap:D_{3d})	tail, 216, 245, 339, 363	<13 100	>18 700	13
YBO_3	(8:237)	(2ctap:C_{3i})	tail, 219, 245, 338, 357	<13 300	>17 600	14,13,12
vaterite-$LuBO_3$	(8:233)	(2ctap:D_{3d})	tail, 218, 239, 346, 365	<13 200	>18 500	12
calcite-$LuBO_3$	(6:224)	(octa:C_{3i})	(180-200), 303, (325), 340			12
$ScBO_3$	(6:212)	(octa:C_{3i})	–, –, 320, (343), 358			14,15
$Lu_2Si_2O_7$	(6:223)	(tap:C_2)	193, 213, (278), 313, 351	12 400	23 300	this work
$La_{9.33}\square_{0.67}(SiO_4)_6O_2(4f)$	(9:259)	(3ctp:C_3)	–, –, –, –, 285	(10 900)	(10 500)	27
$Lu_2SiO_5(Ce_1)$	(7:231)	(irreg:C_1)	(205, 215), 267, 296, 356	12 300	20 700	46

[a]R_{av} was assumed to be 2 pm larger than that in $K_3Ce(PO_4)_2$.
[b]R_{av} was assumed to be 2 pm smaller than that in $La(C_2H_5SO_4)_3\times 9H_2O$.
[c]R_{av} was assumed 14 pm smaller than in $LaMgB_5O_{10}$.
[d]The same R_{av} was assumed as in $Li_6Ho(BO_3)_3$.
[e]R_{av} was assumed 4 pm smaller than in $YAl_3(BO_3)_4$.

III. DISCUSSION

First the observed crystal-field splitting will be related to the type of anion polyhedron coordinating the Ce^{3+} ion. It will be compared with that found in compounds treated in Part I and Part II. Next, centroid shift will be analyzed by means of the ligand polarization model from which the spectroscopic polarizability α_{sp} will be obtained. Finally, ideas on centroid shift and crystal-field splitting are combined to discuss redshift values.

A. Crystal-field splitting

For the interpretation of the crystal-field splitting of Ce^{3+} 5d levels, the same procedures as outlined in Part II will be used. It suffices to consider the first anion coordination polyhedron around Ce^{3+}. Such polyhedron often consists of a prismatic part containing $2m$ anions with an m-fold axis of symmetry (z axis). The faces of the prism can be capped by p anions on the symmetry axis (axial ligands), or/and n anions in the x-y plane perpendicular to it (equatorial ligands).

If all bond lengths from Ce^{3+} to the anions are equal then by means of the point-charge electrostatic model (PCEM) of crystal-field interaction, generalized expressions for the B_q^k crystal-field parameters can be derived (see Ref. 6). Of special interest is the B_0^4 parameter which can be written as

$$B_0^4 = f(R)\left[p + \frac{3n}{8} + \frac{m}{4}(35\cos^4\theta_{pr} - 30\cos^2\theta_{pr} + 3)\right]. \quad (4)$$

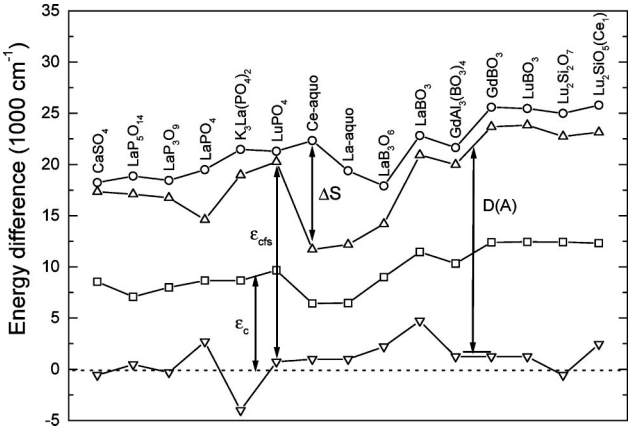

FIG. 3. Energy differences between the centroid position (51 230 cm^{-1}) of the free Ce^{3+} ion and; (∇) highest $5d$ level, ($\square$) centroid energy, ($\triangle$) lowest $5d$ level, and ($\bigcirc$) relaxed lowest $5d$ level of Ce^{3+} in complex oxide compounds.

The function $f(R)$ will be referred to as the radial part. The expression between square brackets is then the angular part Θ_0^4 where the prismatic angle θ_{pr} is the angle the $2m$ ''prismatic'' Ce^{3+}-oxygen bonds make with the m-fold axis. The effect of the shape of the coordination polyhedron on B_0^4 is fully determined by this angular part. The effect of the size is in the radial part. The PCEM predicts that $f(R)$ is proportional to R^{-5}. However, experimentally such dependence is not observed and in that respect the PCEM does not provide an adequate description of crystal-field splitting. It appears though, from the work in Part II, that the angular part is still of value. The functional form of $f(R)$ will be determined empirically from the observed crystal-field splitting.

Figure 4 shows ϵ_{cfs} against $(R_{av}-0.5\Delta R)$ of oxides in Table I, of halides from Part I and Part II, and of new data on $LaBr_3:Ce^{3+}$. In Part I, only four $5d$ levels were reported for $KMgF_3:Ce^{3+}$. Own measurements have revealed the missing fifth excitation band at 196 nm yielding ϵ_{cfs} $=8300$ cm^{-1}. ϵ_{cfs} for $LuCl_3:Ce^{3+}$ is also different from that reported in Part II because, instead of 196 nm, the highest $5d$ level is located at 210 nm.

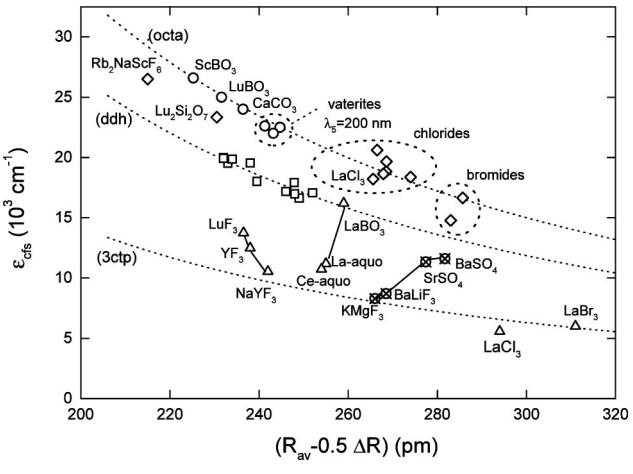

FIG. 4. Crystal-field splitting ϵ_{cfs} of Ce^{3+}. $\diamond$: compounds with (distorted) octahedral coordination; $\square$: compounds with dodecahedral coordination; $\otimes$: compounds with 12-fold coordination; $\triangle$: compounds with ninefold coordination; $\bigcirc$: values estimated in this work.

$0.5\Delta R$ is like in Eq. (3) meant to roughly correct for lattice relaxation around Ce^{3+}. Values for ΔR were obtained from the compilation of ionic radii by Shannon.[7] The so-called crystal radius (CR) pertaining to the appropriate coordination number was used. The dashed curves have the functional form βR^{-2} with $\beta_{octa}=1.35\times10^9$ $pm^2\,cm^{-1}$, $\beta_{ddh}=0.79\beta_{octa}$, and $\beta_{3ctp}=0.42\beta_{octa}$.

1. Tricapped trigonal prism and cuboctahedral coordination

In Part II it was found that for many polyhedrons with threefold symmetry axis, ϵ_{cfs} scales proportionally with the absolute value for Θ_0^4. Θ_0^4 is particularly small (1.15) in the case of ninefold coordination in the form of a regular tricapped trigonal prism (3ctp) as in $NaYF_3$, $LaCl_3$, and $LaBr_3$ with $(p:n:m:\theta_{pr})=(0:3:3:\approx42°)$. The contribution to the crystal-field by the ligands of the trigonal prism is for a large part cancelled by the contribution from the three equatorial ones resulting in small crystal-field splitting. The same holds for 12-fold cuboctahedral (cubo) coordination as in the cubic perovskites $BaLiF_3$ and $KMgF_3$ with $(p:n:m:\theta_{pr})=(0:6:3:35.3°)$. $\Theta_0^4=-1.17$ which is apart from the sign practically the same as for (3ctp) coordination. Figure 4 shows that ϵ_{cfs} for these fluorides falls indeed very close to the curve pertaining to (3ctp) coordination.

The name aquocompounds is used for compounds where the lanthanide ion is fully coordinated by neutral H_2O molecules. Aqueous-$[Ce(OH_2)_9]^{3+}$ (Ce-aquo) is a solution of Ce^{3+} in water. As in Ce^{3+}-doped $La(C_2H_5SO_4)_3\times9H_2O$ (La-aquo), the Ce^{3+} ion is coordinated by nine water molecules in the form of a (3ctp) polyhedron. Crystal-field splitting in these compounds is relatively small, yet the data fall significantly above the curve pertaining to (3ctp) coordination. For $La(C_2H_5SO_4)_3\times9H_2O$, the tricapped trigonal prism is distorted in two respects (i) $\theta_{pr}=47°$ and (ii) the bond lengths to the three caps are 9 pm larger than to the prismatic anions. Both deviations tend to enhance crystal-field splitting. Naively applying Eq. (4) to both the prismatic $(n=p=0)$ and the equatorial ligands $(m=p=0)$ separately and assuming an R^{-2} radial dependence on bond length yields a B_0^4 parameter 20% larger than in the case of a perfectly regular (3ctp). This is about the deviation of the observed crystal-field splitting from the dashed curve in Fig. 4.

The (3ctp) coordination becomes increasingly more distorted in going from $NaYF_4$, to YF_3, and to LuF_3, which is like in the aquocompounds probably the reason for the enhanced crystal-field splitting in these materials. Coordination is ninefold around the La site in the aragonite structure of $LaBO_3$. It is very irregular and La-O distances range from 238 to 280 pm.[8] Figure 4 shows that ϵ_{cfs} is much larger than in the case of (3ctp)-ninefold coordination. Also the 12-fold coordination in $SrSO_4$ and $BaSO_4$ is irregular with varying bond lengths to the central cation. Figure 4 shows that ϵ_{cfs} is much larger than that typical for 12-fold cuboctahedral coordination. These three examples demonstrate that the topological arrangement of the ligands around the Ce^{3+} site is

TABLE II. Spectroscopic and crystallographic properties of scheelites, zirconates, and anhydrites with (ddh) type of coordination. Redshift $D(A)$ and Stokes shift ΔS are from Ref. 2. Predicted values for $ScPO_4$ are within brackets.

Compound	$(\theta_{el}:\theta_{sq}:R_{el}/R_{sq})$	$D(A)$ (cm^{-1})	ΔS (cm^{-1})	ϵ_{cfs} (cm^{-1})	$r(A)$	ϵ_c (cm^{-1})
$LiYF_4(S_4)$	(38°:67°:1.024)	15 300	1600	19 500	1.68	5520
$LiLuF_4(S_4)$		15 100	1240	20 000	1.75	5610
$YPO_4(D_{2d})$	(31°:76°:1.032)	17 700	1670	18 000	1.79	9570
$LuPO_4(D_{2d})$	(31°:76°:1.039)	18 100	1020	19 500	1.89	9670
$ScPO_4(D_{2d})$	(32°:77°:1.054)	19 000		(19 400)	(1.85)	(10 400)
$CaSO_4$ (C_2 or D_2)	$(\approx 28°:\approx 76°:\approx 1.06)^a$	15 400	800	17 900	2.05	8540

[a]Several slightly different structures are reported for the anhydrite structure of $CaSO_4$. Average values are given.

important for ϵ_{cfs}. Ninefold or twelvefold coordination does not automatically guarantee small crystal-field splitting.

In Part II and in Ref. 9 it was noticed that whenever crystal-field splitting is very small, the Stokes shift tends to be very large. This can be observed in Fig. 3 for $LaPO_4$, LaB_3O_6, and in the two aquocompounds. The abnormally large Stokes shift (10 600 cm^{-1}) in aqueous $[Ce(OH_2)_9]^{3+}$ has a special reason. It is caused by the dissociation of one water molecule after Ce^{3+} is brought to its excited 5*d* configuration. The eight remaining water molecules will rearrange into an eightfold polyhedron, possibly a cube or a square antiprism. According to Kaizu *et al.*[10] crystal-field splitting may increase to about 22 000 cm^{-1} resulting in a large Stokes shift.

2. Eightfold dodecahedral (ddh) coordination

An interesting analogy exists between the spectroscopic and crystallographic properties of scheelites ($LiYF_4$,$LiLuF_3$), zirconates (YPO_4,$LuPO_4$), and anhydrites ($CaSO_4$) compiled in Table II. In all three structure types, the small cation (Li^+,P^{5+},S^{6+}) is tetrahedrally coordinated by four anions. The large cation has eightfold coordination. The coordinating polyhedron can be described as that of two interpenetrating tetrahedra. In a cube both tetrahedra are regular and identical with prismatic ($m=2$) angle equal to the cubic angle ($\theta_c=54.7°$). In the scheelites one tetrahedron is strongly elongated ($\theta_{el}<\theta_c$) and the other is squad ($\theta_{sq}>\theta_c$). It results in a polyhedron with 12 triangular faces (dodecahedron) and S_4 site symmetry. A small distortion reduces the symmetry to D_{2d} as in the crystals of the zircon (xenotime) type. The bond lengths to the anions of the elongated tetrahedron (R_{el}) are longer than those to the squatted one (R_{sq}). Values for the prismatic angles and the ratio in bond lengths are compiled in Table II. The dodecahedron (ddh) in $CaSO_4$ is further distorted until C_2 or D_2 site symmetry and there are possibly four different bond lengths.

Crystal-field splitting in the scheelites, zirconates, and $CaSO_4$ with (ddh)-type of coordination is shown in Fig. 4. Also that of LaP_5O_{14}, CeP_5O_{14}, LaP_3O_9, Li_6YBO_3, and that of BaY_2F_8 and $BaLu_2F_8$, see Part I and II, are shown. All six compounds have (ddh) coordination with very low point symmetry. One observed that despite different types of anions involved, ϵ_{cfs} values fall close to the dashed curve with a $\beta_{ddh}R^{-2}$ dependence. Apparently, whether the anion is an oxygen or a fluorine ion is not of much influence for the crystal-field splitting. It is also concluded that deviations from the regular dodecahedron do not influence ϵ_{cfs} much. This is quite contrasting with the situation for (3ctp) and (cubo)coordination where crystal-field splitting does appear quite sensitive to polyhedral distortion.

$ScPO_4$ has like $LuPO_4$ and YPO_4 the zircon-type structure. Based on the $\beta_{ddh}R^{-2}$ dependence, ϵ_{cfs} can be estimated. Centroid shift is then obtained from the known redshift by assuming $r(A)\approx 1.85$; see Table II.

3. Distorted cubal coordination

Some confusion on the (pseudo)vaterite crystal structure of $GdBO_3$, YBO_3, and $LuBO_3$ was solved by Chadeyron *et al.*[11] Coordination around the rare-earth cation is eightfold in the form of a trigonal antiprism capped with two axial ligands (2ctap). It resembles a cube viewed along its body diagonal. For $LuBO_3$, the antiprism (6:238) is elongated from the cubic value of $\theta_{pr}=70.5°$ to $\theta_{pr}=65°$. The two axial ligands, each randomly occupying one of three possible sites, are located at 20 pm closer distance (R_a) than the six prismatic ones (R_{pr}). Furthermore their possible sites are located off axis by $\theta_a=2°$. The values on θ_{pr}, θ_a, and the ratio R_a/R_{pr} for the other compounds can be found in Table III.

The excitation spectra of Ce^{3+} luminescence for each of the crystals with the vaterite structure appear quite similar. Two partly overlapping excitation bands can be distinguished at long wavelengths well separated from two others at short wavelengths.[12,13] A ''tail'' in the spectra extends to beyond 190 nm. Unfortunately, the location of the fifth excitation band is not known, but since three bands are expected to originate from the high energy t_{2g} states of the cubic crystal-field splitting, a location within the tail is well possible. Assuming that the wavelength λ_5 of the fifth 5*d* level is shorter than λ_4, upper and lower limits on ϵ_c and ϵ_{cfs} can be given; see Table I.

Table III shows values for ϵ_c and ϵ_{cfs} obtained assuming a value of 200 nm for λ_5. With this choice, crystal-field splitting for the vaterite phase falls close to that typical for octahedral coordination; see Fig. 4. For ideal cubal coordination

TABLE III. Crystallographic and spectroscopic properties of borates with the vaterite and calcite structure. Values assumed for λ_5, $r(A)$, and ϵ_{cfs} are within brackets.

Compound	$(\theta_{pr}:\theta_a:R_a/R_{pr})$	$D(A)$ (cm^{-1})	λ_5, λ_4 (nm)	ϵ_{cfs} (cm^{-1})	$r(A)$	ϵ_c (cm^{-1})
Vaterite						
$GdBO_3$	(64.0°:3°:0.909)	21 800	(200), 216	22 500	1.99	12 400
YBO_3	(64.4°:19°:0.973)	21 300	(200), 219	22 000	2.04	12 400
Vat-$LuBO_3$	(65°:2°:0.918)	21 900	(200), 218	22 600	1.98	12 400
Calcite						
Calc-$LuBO_3$	$\theta_{pr}=53°$	19 900	184, 194	(25 000)	(2.4)	11 400
$ScBO_3$	$\theta_{pr}=53.4°$	21 400	183, 192	(26 600)	(2.4)	12 200
$CaCO_3$	$\theta_{pr}=52.9°$	17 400	179, 218	(24 000)	(2.4)	9300

PCEM predicts a value 0.89 times that for octahedral coordination; see Part II.

4. Sixfold trigonal prism (tp) and trigonal antiprism (tap) coordination

The PCEM predicts for sixfold octahedral $(p:n:m:\theta_{pr})=(0:0:3:54.7°)$ coordination $\Theta_0^4=-2.33$ and crystal-field splitting is anticipated a factor of 2 larger than for (3ctp) and (cubo)coordination, see Part II. In Fig. 4 the difference appears as a factor of 2.4. Octahedral or (tap) coordination is found in the calcite phases of $LuBO_3$, $ScBO_3$, and $CaCO_3$. In all three compounds, the prismatic angle θ_{pr} is close to 53° which is slightly smaller than that in the perfect octahedron ($\theta_{pr}=54.7°$). One expects to observe three excitation bands at low energy stemming from the t_{2g} triplet levels and two high-energy e_g-type levels. Structural and spectroscopic properties of the three calcite compounds can be found in Table III. For all three crystals, indeed three low-energy excitation bands have been observed; see Table I.

In calcite $LuBO_3:Ce^{3+}$, Zhang observes a weak unresolved band between 180 and 200 nm which may be caused by the e_g type of bands.[12] The location of the two high-energy excitation bands in $CaCO_3$ is not known. $ScBO_3:Ce^{3+}$ has been studied by Blasse and co-workers[14,15] and Hoshina and Kuboniwa.[16] The bands at 358 and 320 nm and possibly a third one at 343 nm were attributed to the t_{2g} levels.[14] Two additional (weak) excitation bands at 260 and 277 nm reported by Blasse *et al.* were assigned to the high-energy e_g levels.[15] However, unrealistic values for both ϵ_c and ϵ_{cfs} are then obtained. Apparently these bands, that were not observed by Hoshina and Kuboniwa, are of different origin.

In the three calcite crystals, one may estimate the total octahedral crystal-field splitting and therewith the wavelength of the highest excitation band λ_5 by employing the $\beta_{octa}R^{-2}$ relationship. By choosing a value for $r(A)=2.4$ typical for octahedral coordination, with Eq. (1), centroid shift is obtained. The location λ_4 can then also be calculated. The thus anticipated values are shown in Table III. Note that those for calcite-$LuBO_3$ agree with the weak unresolved excitation bands observed by Zhang[12] between 180 and 200 nm.

In $Lu_2Si_2O_7$ coordination around the Lu site is distorted octahedral with C_2 point symmetry. Large crystal-field splitting is indeed observed, data falls in the proximity of the upper dashed curve in Fig. 4.

5. Other types of coordination

The aluminumborates $RAl_3(BO_3)_4$ ($R=$Gd, Y, Lu) have the huntite crystal structure with 12-fold coordination around the rare-earth site. Taking $GdAl_3(BO_3)_4$ as a representative, the six closest oxygen ions (6:234) form a trigonal prism with prismatic angle $\theta_{pr}=54°$ which is quite close to the cubic angle 54.7° of the octahedron. The prism is twisted, i.e., the lower triangular face is rotated relative to the upper one. The six more distant oxygen ions (6:307) form again a twisted trigonal prism with prismatic angle $\theta_{pr}=67°$. The crystal structure of $YAl_3(BO_3)_3$, determined by Meszaros *et al.*,[17] is almost identical. All bond lengths to the nearest anions are about 4 pm smaller in accordance with the difference in ionic radius between Y^{3+} and Gd^{3+}. For the same reason the bond lengths in $LuAl_3(BO_3)_3$ are estimated as 4 pm smaller than in the yttrium variant. In Table I $(N:R_{av})$ of both the six closest and six more distant oxygen ions are given.

For a trigonal prism with prismatic angle close to the cubic angle similar crystal-field splitting as for octahedral coordination is expected, see Part II. Based on the inner prism alone, for $GdAl_3(BO_3)_4$ this would imply a value around 24 000 cm^{-1}. However actual crystal-field splitting is more than 5000 cm^{-1} smaller. Probably, the larger (outer) prism cancels part of the crystal field produced by the inner one. This situation is somewhat similar to tricapped trigonal prism and cuboctahedral coordination discussed above.

The tenfold coordination in $LaPO_4$, LaB_3O_6, $LaMgB_5O_{10}$, GdB_3O_6, $YMgB_5O_{10}$ is too irregular to analyze by means of PCEM. Crystal-field splitting falls in between values typical for tricapped trigonal prism and dodecahedral coordination. Coordination in $K_3La(PO_4)_2$ and Lu_2SiO_5 is sevenfold in the form of an irregular polyhedron. In the case of $K_3La(PO_4)_2$ there are two additional ligands at 320 pm. Crystal-field splitting for both compounds falls in between that typical for dodecahedral and octahedral coordination. Note, for sevenfold coordination in the form of a

regular monocapped trigonal prism, $\Theta_0^4 = -2.16$ also falls in between that of (octa) and (ddh) coordination, see Part II.

6. Conclusions on the crystal field splitting

Summarizing, the following conclusions and observation were made. (i) Provided that bond lengths remain constant, crystal-field splitting depends on the polyhedral shape. For several polyhedral types with a threefold axis of symmetry, crystal-field splitting is roughly in accordance with predictions based on the angular part of the B_0^4 crystal-field parameter calculated by the PCEM. (ii) Provided that polyhedral shape remains constant, crystal-field splitting depends roughly as R^{-2} on the average distance to the ligands. (iii) There are no indications that the chemical properties of the anions are of much significance for the crystal-field splitting. (iv) There are no indications that the charge state (neutral in the case of H_2O, -1 for the halides, and -2 for O^{2-}) of the anions is of significance for the crystal-field splitting. (v) The main influence of the type of anion on crystal-field splitting has to do with its ionic radius increasing along the series F^-, O^{2-}, Cl^-, Br^-. It determines the size of the polyhedron and therewith the magnitude of crystal-field splitting.

B. Centroid shift and spectroscopic polarizability

Results on α_{sp} calculated by means of Eq. (2) together with R_{eff} and the contribution to the observed centroid shift per coordinating anion, are compiled in Table IV. For $ScPO_4$ and the compounds with the calcite and the vaterite structure, α_{sp} was calculated adopting the values in Tables II and III.

For the halide compounds it was found in Part I and Part II that α_{sp} is firstly determined by the type of anion. It increases substantially in going from fluorides to chlorides to bromides, for example 0.94, 6.48, and 11.1 $Å^3$ for LaF_3, $LaCl_3$, and $LaBr_3$ respectively. It was also found that α_{sp} scales with the ionic radius and the valency of the cations that coordinate the anion ligands. The smaller the cations and the more abundant they are, the smaller α_{sp} tends to be.

Table IV shows that the same principle applies for the oxide compounds. In the series LaP_5O_{14}, LaP_3O_9, $LaPO_4$, and $K_3La(PO_4)_2$, the small phosphor cation abundance decreases and α_{sp} increases steadily. Replacing La^{3+} in $LaPO_4$ by the smaller Y^{3+} or even smaller Lu^{3+} reduces α_{sp}. Amongs the borates, α_{sp} is smallest for the metaborate $YMgB_5O_{10}$ containing a high abundance of B^{3+} cations. α_{sp} is also small for $LuAl_3(BO_3)_4$ containing the small trivalent cations B^{3+}, Al^{3+}, and Lu^{3+}. α_{sp} in $LaBO_3$ with the large fraction of relatively large La^{3+} and in $Li_6Y(BO_3)_3$ with a large number of monovalent Li^+ cations is largest. α_{sp} decreases in the series $LaBO_3$, $GdBO_3 \approx YBO_3$, $LuBO_3$, $ScBO_3$ with decreasing size of the rare-earth ion.

Clearly the spectroscopic polarizability is intimately connected with the chemical bonding of the oxygen ligands within the inorganic compound. This is also revealed in Fig. 5 where α_{sp} for La-based oxide compounds is shown against the compound identification number. These compounds were selected because relaxation around Ce^{3+} on the La site will be minimal and the local environment around Ce^{3+} is known with least uncertainty. The error in α_{sp} will then be small. A fair estimate for Ce^{3+} on a site exclusively coordinated by SiO_4^{4-} ortho type of complexes will be made for $La_{9.33}(SiO_4)_6O_2$ in Sec. III C. This data is also shown in Fig. 5. The values for $CaSO_4$ and $CaCO_3$ are shown because ΔR for Ce^{3+} on a Ca site is also very small.

A clear pictures emerges if one connects the data belonging to the ortho type of compounds, starting from $CaSO_4$ via $CaCO_3$, $LaPO_4$, $LaBO_3$ to $La_{9.33}(SiO_4)_6O_2(4f)$. Along this series there is a tendency of increasing value for the polarizability which is related with decreasing binding strength of the oxygen ions within the ortho type of complexes. Figure 5 also shows that within the phosphates and borates, α_{sp} increases with decreasing amount of condensation between the complexes. A neutral water molecule provides a very small value for α_{sp}. It leads to the conclusion that the oxygen ligands are strongly bonded to the two hydrogen atoms within the molecule and interaction with the Ce^{3+} 5*d* electron either by means of polarization or covalency is minimal.

TABLE IV. Results from the ligand polarization model. In this work predicted values are within brackets.

Compound	R_{eff} (pm)	ϵ_c/N (cm^{-1})	α_{sp} (10^{-30} m^3)
$CaSO_4$	247	1070	1.68
$SrSO_4$	272	660	1.83
$BaSO_4$	278	660	2.10
$CaCO_3$	236	(1550)	$\approx$1.88
CeP_5O_{14}	248	900	1.45
LaP_5O_{14}	249	880	1.45
$ScPO_4$	234	(1300)	$\approx$1.49
$LuPO_4$	238	1210	1.53
YPO_4	240	1200	1.57
LaP_3O_9	249	1000	1.66
$LaPO_4$	259	870	1.81
$K_3La(PO_4)_2$	257	960	1.91
Aqueous $[Ce(OH_2)9]^{3+}$	254	710	1.33
$La(C_2H_5SO_4)_3 \times 9H_2O$	255	720	1.36
$YMgB_5O_{10}$	258	730	1.47
$LuAl_3(BO_3)_4$	244	840	1.60
GdB_3O_6	254	900	1.68
$YAl_3(BO_3)_4$	257	850	1.71
$LaMgB_5O_{10}$	265	750	1.78
$GdAl_3(BO_3)_4$	259	860	1.79
$ScBO_3$	225	(2030)	$\approx$1.84
LaB_3O_6	258	900	1.85
Calc-$LuBO_3$	232	(1900)	$\approx$2.04
Vat-$LuBO_3$	240	(1550)	$\approx$2.07
YBO_3	243	(1550)	$\approx$2.23
$GdBO_3$	243	(1550)	$\approx$2.22
$LaBO_3$	254	1270	2.38
$Li_6Y(BO_3)_3$	245	(1590)	2.4$\pm$0.2
$Lu_2Si_2O_7$	230	2070	2.15
$Lu_2SiO_5:(Ce_1)$	238	1760	2.22
$La_{9.33}\square_{0.67}(SiO_4)_6O_2(4f)$	256	(1210)	2.4$\pm$0.2

Note, however, that it is still larger than the value of 0.94 $Å^3$ for LaF_3.

C. Spectroscopic redshift

Data presented in Fig. 1 show that variation of the redshift values within a group of compounds like the borates or phosphates is larger than the variation between groups, and at first sight no apparent trend is observed. The aim of the following discussion is to closely investigate the redshift in relation to the crystal structure and physical and chemical properties of the atoms in the compounds. The seemingly random scattering of the data in Fig. 1 turns out to behave quite orderly. We will start with the data on the sulfates and proceed from left to right through Fig. 1 to the silicates.

1. Sulfates and carbonates

The data on the oxyorthosulfates in Fig. 1 pertain to $La_2O_2(SO_4)(8{:}258)$, $Gd_2O_2(SO_4)(8{:}247)$, and $Y_2O_2(SO_4)(8{:}244)$. Redshift is about 3600 cm^{-1} larger than in $CaSO_4(8{:}247)$. There are four oxygen ions in the coordination sphere around the rare-earth site that are not bonded in a sulfate complex. These so-called oxyanions are expected to contribute relatively strongly to α_{sp} resulting in larger centroid shift than in $CaSO_4$. It is not expected that ϵ_{cfs} in the oxyorthosulfates will be much different from that in $CaSO_4$.

Information on fd transitions in the carbonates is very scarce. Besides in the calcite structure, $CaCO_3$ also exists in the vaterite structure. From the work by Kojima *et al.*,[18] a redshift 900 cm^{-1} larger than in the calcite phase is obtained. Data near 15 500 cm^{-1} in Fig. 1 belong to $Ce_2(CO_3)_3$ and $La_2(CO_3)_3$.

2. Phosphates

The values for the redshift known in the phosphate compounds can be seen in Fig. 6. On the left, the compounds with high degree of condensation of the PO_4^{3-} complexes can be found. From LaP_5O_{14}, CeP_5O_{14}, $PrP_5O_{14}(8{:}246)$, to TbP_5O_{14}, redshift increases with smaller size of the lanthanide ion. Although the crystal structure is not the same for all four compounds, it is most likely caused by an increase of crystal-field splitting. For the same reason the metaphosphates LaP_3O_9, $GdP_3O_9(6{:}228)$, and $YP_3O_9(6{:}224)$ show increase of redshift with smaller size of the rare-earth ion and decreasing coordination number. The data for LaP_5O_{14}, LaP_3O_9, and $LaPO_4$ have been connected by line segments. As can be seen in Fig. 3, the increase of centroid shift with smaller degree of condensation is more than compensated by the reduction in crystal-field splitting in going from LaP_5O_{14} to $LaPO_4$.

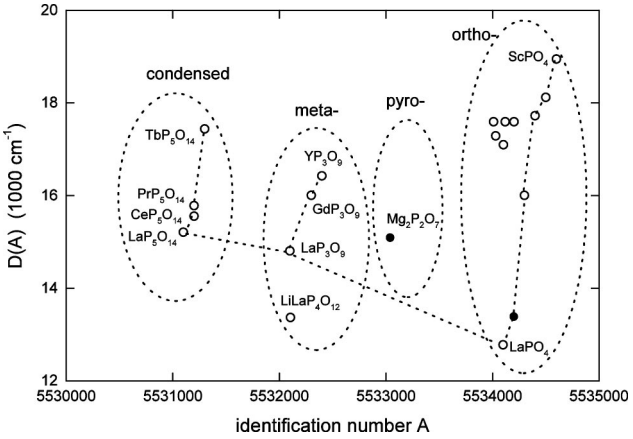

FIG. 6. Redshift in phosphate compounds. ●: redshift values estimated from df emission wavelengths.

Figure 7 is a ten times expanded view of part of Fig. 6. On this scale the fifth digit of the identification number is of significance. It indicates the type of rare-earth cation in the host crystal. On the far left with $d_5=0$, the compounds lacking rare-earth cations can be found, i.e., $Ca_3(PO_4)_2$ and $Ba_4SO_4(PO_4)_2$. For compounds containing La, Ce, Gd, Y, Lu, or Sc, $d_5=1$, 2, 3, 4, 5, or 6, respectively. Size of the rare-earth cation decreases in that order and crystal-field splitting tends to increase. This is nicely demonstrated by the series of compounds starting from $LaPO_4$ to $ScPO_4(8{:}221)$. $CePO_4(10{:}262)$ and $GdPO_4(10{:}255)$ have like $LaPO_4(10{:}264)$ the monazite structure. The others are of the

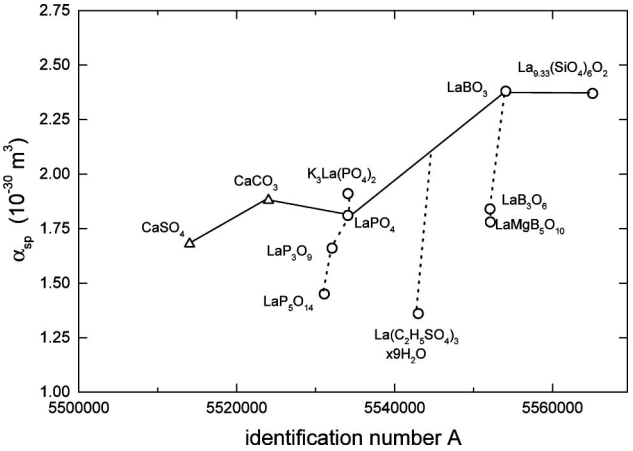

FIG. 5. Spectroscopic polarizability of La- and Ca-based compounds.

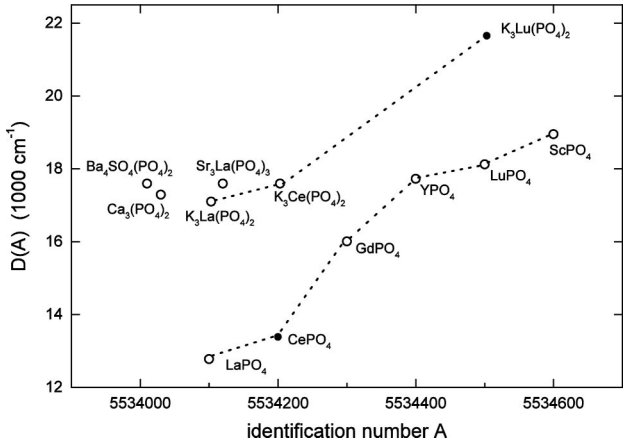

FIG. 7. Redshift in the orthophosphate compounds. ●: redshift values estimated from df emission wavelengths.

zircon (xenotime) type; see Table II. The same is demonstrated by the series of compounds $K_3La(PO_4)_2$(7:252), $K_3Ce(PO_4)_2$(7:249) and $K_3Lu(PO_4)_2$(6:220). Compared to the $LaPO_4$, $CePO_4$, and $LuPO_4$ redshift has increased for each compound by about 4000 cm^{-1}. Redshift values in several other $M_xLa(PO_4)_y$ with M an alkaline or alkaline-earth cation are known. Only that of $Sr_3La(PO_4)_3$(7:261) is shown in Fig. 7, the other values in Ref. 2 do not significantly differ.

In the discussion on the fluorides in Part I, it was found that addition of large cations in the structure tends to enhance redshift. Two reasons were mentioned: (i) large cations increase the polarizability of the anions and thus increase the centroid shift, and (ii) large cations tend to reduce the coordination number around the lanthanide and this has the tendency to increase crystal-field splitting. Coordination number in the rare-earth phosphates indeed decreases when the large K^+ cations are present. For $K_3La(PO_4)_2$ centroid shift and crystal-field splitting is significantly larger than in $LaPO_4$. Other orthophosphates with large cations like Ba^{2+}, Sr^{2+} and Na^+ also show, probably for the same reasons, relatively large redshift.

3. Hydrated compounds and aquocompounds

Apart from the two aquocompounds, all data in Fig. 1 pertain to hydrated orthosulfates, and Ce^{3+} has both H_2O molecules and SO_4^{2-} complexes in its coordination sphere. Redshift in the hydrated sulfates is typically 5000 cm^{-1} larger than that in the aquocompounds. Since the contribution from H_2O to α_{sp} is small, replacing H_2O molecules by SO_4^{2-} complexes will tend to enhance α_{sp}. An enhanced contribution from ϵ_c to the redshift is anticipated.

4. Borates

(a) *Condensed borates.* In the condensed borates, the triangular (BO_3^{3-}) or tetrahedral (BO_4^{5-}) borate groups are linked by corner or edge sharing of oxygen ions into two- or three-dimensional networks. Covalence within the networks will be large and one expects a relatively small value for α_{sp} and ϵ_c. The values for the redshift can be found in Fig. 2.

In $SrB_4O_7:Ce^{3+}$ two different Ce centers have been observed.[19] The site showing the smallest value for the redshift (14 100 cm^{-1}) was attributed to an isolated Ce^{3+} ion on a Sr^{2+} site without local charge compensation. This site has nine ligands at relatively close distance (9:263) plus three more distant ones. Redshift is of the same largeness as in the metaborates, and probably the centroid shift and crystal-field splitting are comparable also. The other Ce site shows a 4000-cm^{-1} larger redshift. It has been attributed to Ce^{3+} centers locally charge compensated by means of a Sr^{2+} vacancy.[19] A quite similar situation was encountered for $CsCdBr_3:Ce^{3+}$; see Ref. 20. The presence of a cation vacancy as charge compensator enhances the redshift by several 1000 cm^{-1}. One reason for the relatively large redshift may be an enhanced crystal-field splitting due to relaxation of oxygen ions towards Ce^{3+}. A cation vacancy is also thought to enhance centroid shift since a binding with the oxygen ligands is absent resulting in relatively large polarizability. Cation vacancies may also be present in CaB_4O_7. In SrB_6O_{10} studied by Koskentalo *et al.*,[21] two different Ce^{3+} sites were identified. Redshifts are quite similar as for the two sites in SrB_4O_7.

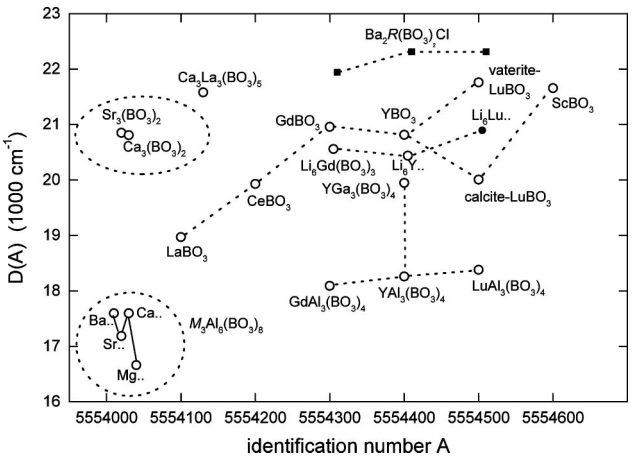

FIG. 8. Redshift in the orthoborate compounds and the chloro-orthoborates $Ba_2R(BO_3)Cl$. For displaying purposes, the second digit of the identification number of the chloroborates was changed from 2 to 5.

(b). *Metaborates and pyroborates.* The metaborates were already fully discussed in previous sections. On the pyroborates, only the spectroscopic properties of Ce^{3+} doped $Sr_2B_2O_5$ are known.[22] Compared to SrB_4O_7 redshift has increased by 6000 cm^{-1}; see Fig. 2. The smaller fraction of boron in $Sr_2B_2O_5$ promotes larger centroid shift and the smaller coordination number, i.e., eightfold instead of nine- to twelvefold for SrB_4O_7, promotes larger crystal-field splitting.

(c) *Orthoborates.* An overview of the redshift in the orthoborates can be seen in Fig. 8. In the chloroborates $Ba_2R(BO_3)_2Cl$ with (R=Gd,Y,Lu), the rare-earth ion is exclusively coordinated by oxygen ions. In that respect they may be treated as orthoborates and the redshifts of these compounds are also incorporated in Fig. 8.

The increase of the redshift with decrease of the rare-earth site size for the RBO_3 compounds (R=La, Ce, Gd, Y, Lu, Sc) is directly related to crystal-field splitting as discussed in previous sections. The vaterite version of $LuBO_3$ has larger redshift than the calcite version. Note, that also the redshift in vaterite $CaCO_3$ was larger than in calcite $CaCO_3$. For $Li_6R(BO_3)_4$, $RAl_3(BO_3)_4$, and $Ba_2R(BO_3)_2Cl$ with R =Gd, Y, Lu, there is no significant increase of redshift with smaller rare-earth size.

The smallest redshifts are found among the aluminum orthoborates of composition $M_3Al_6(BO_3)_6$ (M=Ba, Sr, Ca, Mg). Compared to $Sr_3(BO_3)_2$ and $Ca_3(BO_3)_2$(8:249) the redshifts are more than 3000 cm^{-1} smaller. It was already suggested by Kutty[23,24] that the polarization of the borate groups by the small Al^{3+} ions enhances the ionicity (decreases covalency) between Ce^{3+} and the oxygen ligands. Translated to the ligand polarization model, this is the same as stating that the oxygen ligands are more strongly bonded by the presence of small cations, and the value for α_{sp} is small.

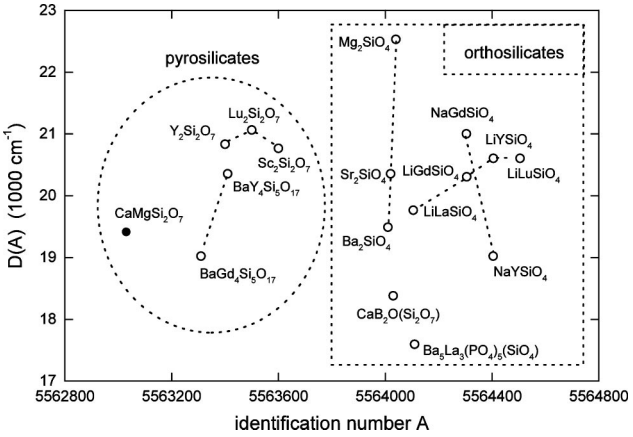

FIG. 9. Redshift in the pyro- and orthosilicate compounds. ●: redshift values estimated from df emission wavelengths.

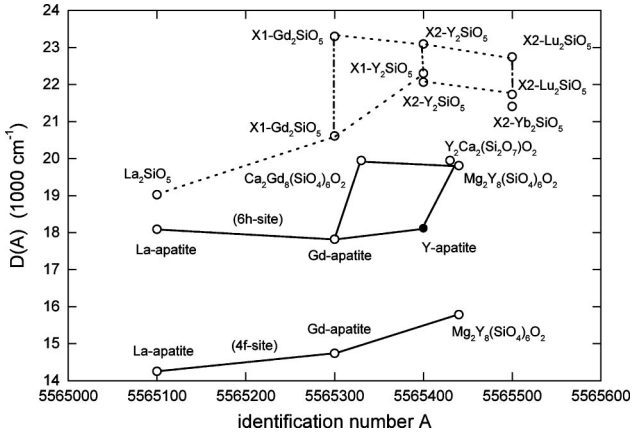

FIG. 10. Redshift in the oxyorthosilicate compounds. ●: redshift values estimated from df emission wavelengths.

In discussing the phosphates, a relationship between the largeness of the redshift and the size of the cations other than the one replaced by Ce^{3+} was mentioned. This phenomenon can also be demonstrated for the yttrium based borate compounds. Going from $Ba_2Y(BO_3)_2Cl$ to $Li_6Y(BO_3)_3$ to $YGa_3(BO_3)_4$ and finally to $YAl_3(BO_3)_4$, the large Ba^{2+} ions in the formula are respectively replaced by Li^+, Ga^{3+}, and Al^{3+} ions. Redshift decreases in the same order. If one inspects the redshifts of the La-, Gd-, and Lu-based compounds similar trends are observed.

(d) *Oxyorthoborates.* The final borate family to be discussed is formed by the oxyorthoborate compounds. These materials may contain isolated BO_4^{5-} or isolated BO_3^{3-} groups together with oxygen ions not bonded to a boron ion. As observed for the oxyorthosulfates, redshifts of the oxyorthoborates are on average several 1000 cm^{-1} larger than those of the orthoborates. It is attributed to the presence of the unbound oxygen ions. They are usually at relatively short distance from the cation and their polarizability is assumed to be large. Both aspects will enhance their contribution to the centroid shift. All the oxyorthoborates in Fig. 2 contain Ca^{2+} or Sr^{2+} alkaline-earth cations. The smallest value for the redshift is observed for $CaAl_2B_2O_7$ and the largest for $CaYOBO_3$.

5. Silicates

The SiO_4^{4-} tetrahedral complexes can like the phosphate and borate complexes condense into the pyro-, meta-, and more condensed structures. The highest degree of condensation is found in SiO_2 where Ce^{3+} can be dispersed within the pores of the silica host. The redshift of 16 000 cm^{-1} from the work by Weiping Cai *et al.*[25] is relatively small for a silicate compound; see Fig. 1.

For the *pyrosilicates*, see Fig. 9, information on centroid shift and largeness of crystal-field splitting is only available for $Lu_2Si_2O_7$; see Table I. Like in $Lu_2Si_2O_7$, the coordination is distorted octahedral in $Y_2Si_2O_7$(6:229)(octa:C_1) and $Sc_2Si_2O_7$(6:212)(octa:C_2). All three compounds show about the same redshift. Apparently, the anticipated larger crystal-field splitting with smaller site size in going from the Y, to Lu, to the Sc variant, is compensated by smaller centroid shift.

(a) *Orthosilicates.* According to Felsche,[26] for stoichiometric reasons, binary orthosilicate compounds exist only with divalent cations like the M_2SiO_4 (M=Ba, Sr, Mg, Be) compounds. For M=Ba, Sr, Mg redshift increases with smaller size of the cation, see Fig. 9. This is mainly attributed to the increase of crystal-field splitting from about 12 500 cm^{-1} for Ba_2SiO_4 to an estimated value of 25 000 cm^{-1} for Mg_2SiO_4(6:214). All other orthosilicates appearing in Fig. 9 are mixed-cation compounds containing monovalent cations like Li^+ or Na^+ and a rare earth ion (La, Gd, Y, Lu). The compounds of composition $LiRSiO_4$ (R=La, Gd, Y, Lu) demonstrate increase of redshift with decrease of the lanthanide size. Redshift in $NaGdSiO_4$ is for unknown reasons relatively large.

(b) *Oxyorthosilicates.* Redshift values of the oxyorthosilicates are shown in Fig. 10. An interesting group of compounds are those with the apatite structure like $La_{9.33}(SiO_4)_6O_2$ (La apatite). In the apatite structure there are two sites for the lanthanide ion.

The Wyckoff $4f$ site is ninefold coordinated, and each oxygen ion belongs to an isolated SiO_4 group forming a (3ctp:C_3) polyhedron. In a way, the $4f$-site can be seen as an orthosilicatelike site. Information on all five $5d$ level energies is not available for this site in the apatites, and crystal-field splitting and spectroscopic polarizability cannot be determined either. Nevertheless, one may attempt to estimate the values for La apatite. With R_{av}-0.5ΔR=259 pm, crystal-field splitting due to the distorted (3ctp) coordination is estimated to be 10 500±1500 cm^{-1}, agreeing more or less with the reflection spectrum reported by Lammers and Blasse.[27] Equation (1) with $D(A)$=14 250 cm^{-1} and $r(A)$ =2.00±0.08, typical for (3ctp) coordination, yields ϵ_c =10 900±800 cm^{-1} and α_{sp}=2.4±0.2 Å^3. This value was used in Fig. 5.

The other rare-earth site in the apatite crystal structure (Wyckoff $6h$) is irregularly coordinated by 9–10 oxygen ligands. Seven of them are at relatively close distance. The nearest oxygen ion (229 pm in La apatite) does not belong to a silicate group. In all three apatites, La apatite(7:249), Gd

apatite(7:241), and the so-called ''2:8 mixed-cation'' apatite $Mg_2Y_8(SiO_4)_6O_2$(7:237), this site has about 4000 cm^{-1} larger redshift than the $4f$ site. Like in the oxysulfates and oxyborates, the short Ln-oxyoxygen bond length and its assumed large polarizability will give an enhanced contribution to the centroid shift. Also the crystal-field splitting is likely to be larger than in the case of the (3ctp) coordination around the $4f$ site.

Bondar *et al.*[28] reported the emission in Ce^{3+}-doped Y apatite. If we assume the same Stokes shift (7300 cm^{-1}) as observed for $Mg_2Y_8(SiO_4)_6O_2$ one obtains a redshift of 18 100 cm^{-1}. Figure 10 shows that data fall in line with expectations based on the $6h$ sites. Therefore the emission is ascribed to Ce on the $6h$ site. The excitation spectrum of Tb^{3+} luminescence in $Ca_2Gd_8(SiO_4)_6O_2$ presented by Jun Lin and Qiang Su[29] shows an allowed fd transition at 235 nm. The corresponding redshift of 19 900 cm^{-1} indicates that this excitation band most probably stems from Tb^{3+} on a $6h$ site.

The last group of compounds to be discussed are the R_2SiO_5 (R=La, Gd, Y, Yb, Lu) type of compounds. They can all be found in the top of Fig. 10 showing relatively large values for the redshift. Interpretation is complicated by the fact that the crystal structure often contains two different lanthanide sites. Furthermore the Gd-based compounds crystallize in the so-called $X1$-type structure and the Yb and Lu compounds have structure type $X2$.[30] For Y_2SiO_5 both phases exist.[26,30]

La_2SiO_5 has probably its own structure type.[31] The redshift in this compound, as deduced from the dipole allowed fd band in Tb^{3+} reported by Leskelä and Suikkanen,[31] is the smallest among the R_2SiO_5 group of compounds. To assign the observed luminescence excitation bands to specific sites in the other compounds, the following three trends will be exploited. (i) Redshift tends to increase with decrease of coordination number, (ii) redshift tends to increase with decrease of site site, and (iii) redshift tends to increase with increase of the number of oxyoxygen ions in the coordination sphere.

The Gd site with the smallest redshift is now assigned to the so-called $A1$-site which is coordinated by nine oxygen ions (9:249). This site resembles the $6h$ site in Gd apatite in a sense that both have one unbound oxygen ion in the ninefold coordination sphere. The other site ($A2$ site) in Gd_2SiO_5 has lower coordination number (seven), smaller size, and three oxyanions yielding 3000 cm^{-1} larger redshift. Both rare earth sites of the Y and Lu compounds with the so-called $X2$-type structure have two unbound oxygen ions in the first coordination sphere. The one with smallest redshift (Ce_1 site) is assigned to the sevenfold coordinated site and the one with largest redshift to the smaller sixfold coordinated one. For the Ce_1 site in Lu_2SiO_5 all five $5d$-level energies are known and Fig. 4 shows that the dominant contribution to the large redshift stems from the large crystal-field splitting.

IV. SUMMARIZING CONCLUSIONS

A. Centroid shift

Within the ligand polarization model, the centroid shift of the $5d$ configuration depends on coordination number, bond lengths, and anion polarizability of the nearest anion neighbors. The spectroscopic polarizability α_{sp} has been calculated without the use of any fitting parameters, from the observed centroid shift. For the halides it was already concluded in Part II that α_{sp} scales with the types of cations present in the compound approximately as follows:

$$Mg^{2+}<Lu^{3+}<Th^{4+}<Y^{3+}<Li^{+}<La^{3+}<Ca^{2+}$$
$$<Na^{+}<Sr^{2+}<Ba^{2+}<K^{+}<Rb^{+}<Cs^{+}<\text{cation vacancy}, \quad (5)$$

where small cations are in the beginning of the series and large cations at the end of the series. Based on the results in this work, this series can be extended to the left by

$$S^{6+}<C^{4+}<P^{5+}<B^{3+}<Si^{4+}<Al^{3+}<Mg^{2+}. \quad (6)$$

The reader may have noticed already the close relationship between the ordering of the cations in the above two series with the Pauling type[32] of electronegativity of the atoms. It follows exactly the same sequence but in reversed order. With smaller electronegativity, the bonding of the valence electrons of oxygen to the metal cation decreases resulting in larger polarizability. Relationship between electronegativity and luminescence properties have been noticed before in the spectroscopy of dd transitions and ff transitions, and based on electronegativity, van Uitert in 1984 proposed a model for the redshift in Ce^{3+} doped materials.[20] However, such model is too crude for practical use, since it does not properly take the crystal-field splitting into account. Relationship with electronegativity is revealed much more clearly when it is applied to the centroid shift and even more clearly when it is applied to the spectroscopic polarizability.

The importance of the anions in determining the value of the centroid shift and spectroscopic polarizability is in the following sequence:

$$\text{anion vacancy}<F^{-}<O^{2-}<Cl^{-}<Br^{-}<I^{-}, \quad (7)$$

where the ''complex'' oxides fall in between the fluorides and chlorides, This sequence follows the actual polarizability of the anions, being smallest for fluorine and largest for iodine. It also follows electronegativity of the atoms, being largest for fluorine and smallest for iodine.

B. Crystal-field splitting

Crystal-field splitting of the $5d$ levels is largely controlled by the nearest anion ligands. Particularly the anion polyhedral shape and size are of importance. Octahedral, dodecahedral, tricapped trigonal prism, and cuboctahedral type of coordination was studied in more detail. For these types of polyhedra, crystal-field splitting scales as $\epsilon_{cfs}=\beta R^{-2}$ with the bond length, i.e., size of the polyhedron. With R in pm and ϵ_{cfs} in cm^{-1}, $\beta_{octa}=1.35\times10^{9}$ $pm^2\,cm^{-1}$ for Ce^{3+}. That of (ddh), (3ctp), and (cubo)coordination are 0.79, 0.42, and 0.42 times that of (octa)coordination, respectively.

For the compounds treated in this work and in Part I and II, no indications were found that either the charge state of the anions (neutral in case of H_2O, -1 for the halides, and

-2 for O^{2-}), or the type of anion (F, Cl, Br, O) is of significance for the crystal-field splitting. For example, if F^- were to be replaced by other halogens, O^{2-}, or H_2O molecules without altering shape and size of the anion polyhedron then crystal-field splitting remains fairly the same also. All data indicate that the crystal-field splitting of Ce^{3+} $5d$ levels behaves independently from the centroid shift. This is a very convenient property since it enables one to interpret both aspects separately from each other as has been done in this work. It also confirms the validity of the approximations made by Morrison[5] leading to the ligand polarization model as expressed by Eq. (2). All five $5d$ levels and therewith the centroid energy are predicted to experience the same shift due to ligand polarization.

[1] P. Dorenbos, J. Lumin. **91**, 91 (2000).
[2] P. Dorenbos, J. Lumin. **91**, 155 (2000).
[3] P. Dorenbos, Phys. Rev. B **62**, 15 640 (2000).
[4] P. Dorenbos, Phys. Rev. B **62**, 15 650 (2000).
[5] C.A. Morrison, J. Chem. Phys. **72**, 1001 (1980).
[6] C. Görller-Walrand and K. Binnemans, *Handbook on the Physics and Chemistry of Rare Earths*, edited by K.A. Gschneidner, Jr. and L. Eyring (Elsevier Science B.V., Amsterdam, 1996), Vol. 23, Chap. 155.
[7] R.D. Shannon, Acta Crystallogr., Sect. A: Cryst. Phys., Diffr., Theor. Gen. Crystallogr. **A32**, 751 (1976).
[8] R.E. Newnham, M.J. Redman, and R.P. Santero, J. Am. Ceram. Soc. **46**, 253 (1963).
[9] P. Dorenbos, J. Andriessen, M. Marsman, and C.W.E. van Eijk, Radiat. Eff. Defects Solids (to be published).
[10] Y. Kaizu, K. Miyakawa, K. Okada, H. Kobayashi, M. Sumitani, and K. Yoshihara, J. Am. Chem. Soc. **107**, 2622 (1985).
[11] C.G. Chadeyron, M. Elghozzi, M. Mahiou, R. Arbus, and J.C. Cousseins, J. Solid State Chem. **128**, 261 (1997).
[12] L. Zhang, Ph.D. thesis, l'Universite Claude Bernard-Lyon I, France, 1997.
[13] A. Mayolet, Ph.D. thesis, Universite de Paris XI Orsay, France, 1995.
[14] G. Blasse and A. Bril, J. Chem. Phys. **47**, 5139 (1967).
[15] G. Blasse, G.J. Dirksen, W.E.J. van Kooten, and C.A. van Walree, Chem. Phys. Lett. **146**, 343 (1988).
[16] T. Hoshina and S. Kuboniwa, J. Phys. Soc. Jpn. **32**, 771 (1972).
[17] Gy. Meszaros, E. Svab, E. Beregi, A. Watterich, and M. Toth, Physica B **276-278**, 310 (2000).
[18] Y. Kojima, K. Machi, T. Yasue, and Y. Arai, J. Ceram. Soc. Jpn. **108**, 836 (2000).
[19] J.W.M. Verwey, G.J. Dirksen, and G. Blasse, J. Phys. Chem. Solids **53**, 367 (1992).
[20] L.G. van Uitert, J. Lumin. **29**, 1 (1984).
[21] T. Koskentalo, L. Niinistö, and M. Leskelä, J. Less-Common Met. **112**, 67 (1985).
[22] V.P. Dotsenko, I.V. Berezovskaya, N.P. Efryushina, A.S. Voloshinovskii, P. Dorenbos, and C.W.E. van Eijk, J. Lumin **93**, 137 (2001).
[23] T.R.N. Kutty, Mater. Res. Bull. **25**, 485 (1990).
[24] T.R.N. Kutty, Mater. Res. Bull. **25**, 343 (1990).
[25] Weiping Cai, Ye Zhang, and Lide Zhang, J. Mater. Res. **14**, 1922 (1999).
[26] J. Felsche, Struct. Bonding (Berlin) **13**, 99 (1973).
[27] M.J.J. Lammers and G. Blasse, J. Electrochem. Soc. **134**, 2069 (1987).
[28] I.A. Bondar, A.A. Kolpakova, L.Ya. Markovskii, A.N. Sokolov, L.E. Tarasova, and N.A. Toropov, Bull. Acad. Sci. USSR, Phys. Ser. (Engl. Transl.) **33**, 977 (1969).
[29] Jun Lin and Qiang Su, J. Alloys Compd. **210**, 159 (1994).
[30] Jun Lin, Qiang Su, Hongjie Zhang, and Shubin Wang, Mater. Res. Bull. **31**, 189 (1996).
[31] M. Leskelä and J. Suikkanen, J. Less-Common Met. **112**, 71 (1985).
[32] L. Pauling, *The Nature of the Chemical Bond* (Cornell University Press, New York, 1960).
[33] E. van der Kolk, P. Dorenbos, A.P. Vink, R.C. Perego, C.W.E. van Eijk, and A.R. Lakshmanan Phys. Rev. B (to be published).
[34] G. Blasse and M. Aguilar, J. Lumin. **29**, 239 (1984).
[35] W. Lenth, Ph.D. thesis, University of Hamburg, Germany, 1979.
[36] B. Blanzat, J-P. Denis, C. Pannel, and C. Barthou, Mater. Res. Bull. **12**, 455 (1977).
[37] M.V Hoffman, J. Electrochem. Soc. **118**, 1508 (1971).
[38] B. Finke, L. Schwarz, P. Gürtler, M. Kraas, M. Joppien, and J. Becker, J. Lumin. **60&61**, 975 (1994).
[39] N.P. Karanjikar and R.C. Naik, Solid State Commun. **65**, 1419 (1988).
[40] R.C. Ropp, J. Electrochem. Soc. **115**, 841 (1968).
[41] G.M. Williams, N. Edelstein, L.A. Boatner, and M.M. Abraham, Phys. Rev. B **40**, 4143 (1989).
[42] K. Okada, Y. Kaizu, H. Kobayashi, K. Tanaka, and F. Marumo, Mol. Phys. **54**, 1293 (1985).
[43] B. Saubat, C. Fouassier, P. Hagenmuller, and J.C. Bourcet, Mater. Res. Bull. **15**, 193 (1981).
[44] M.J. Knitel, P. Dorenbos, C.W.E. van Eijk, B. Plasteig, B. Viana, A. Kahn-Harari, and D. Vivien, Nucl. Instrum. Methods Phys. Res. A **443**, 364 (2000).
[45] O. Aloui-Lebbou, C. Goutaudier, S. Kubota, C. Dujardin, M. Th. Cohen-Adad, C. Pedrini, P. Florian, and D. Massiot, Opt. Mater. **16**, 77 (2001).
[46] I.A. Kamenskikh, V.V. Mikhailin, I.H. Munro, D.Y. Petrovykh, D.A. Shaw, P.A. Studenikin, A.N. Vasil'ev, I.A. Zagumennyi, and Yu.D. Zavartsev, Radiat. Eff. Defects Solids **135**, 391 (1995).